Green Synthesis and Characterization of Silver Nanoparticles from *Vangueria infausta* Leaf Extract for Evaluation of Cytotoxicity in Breast Cancer

Nosipho T. Fakudze[1], Heidi Abrahamse[1] and Blassan P. George[1]*

[1]*Laser Research Centre, Faculty of Health Sciences, University of Johannesburg, P.O. Box 17011, Doornfontein 2028, South Africa.*

ABSTRACT

Green synthesis of silver nanoparticles (AgNPs) using plant extracts offers an eco-friendly alternative to chemical methods, yet the anticancer potential of many medicinal plants remains unexplored. This study explores the biogenic synthesis of silver nanoparticles (AgNPs) from the aqueous extract of *Vangueria infausta* and their cytotoxic effect on breast cancer cells. Synthesised AgNPs were characterised using UV-vis spectrophotometry, scanning electron microscopy (SEM), energy-dispersive spectroscopy (EDS), transmission electron microscope (TEM), and Fourier transform infrared spectroscopy (FTIR). These nanoparticles were further analysed for their mechanisms of cell death and cell viability using flow cytometry and adenosine triphosphate (ATP) measurements. UV-Vis confirmed AgNP formation at 450 nm, revealing circular nanoparticles (17.6 nm) with a silver absorption peak at 3 keV. Colloidal stability was demonstrated by zeta potentials of –29.3 mV (pH 6.6, tumour environment) and –30.6 mV (pH 7.4, physiological state), with hydrodynamic diameters of 172 and 173.7, respectively. FTIR showed functional groups (O-H, C=O, C-H, C=O and C-N) at corresponding absorption bands. These results confirm the successful synthesis of silver nanoparticles from *V. infausta* leaves and highlight their potential as an anticancer agent.

KEYWORDS

Green Synthesis; Silver Nanoparticles; *Vangueria infausta*; Breast Cancer; Cytotoxicity

Received: 3 June 2026 Revised: 13 August 2026 Accepted: 26 August 2026

INTRODUCTION

Cancer poses significant public health, economic, and societal challenges, being responsible for nearly one in six deaths worldwide. It ranks as one of the top three causes of mortality for both men and women aged 30 to 69 in 177 out of 183 countries, contributing to about 30.3% of premature deaths from noncommunicable diseases. In 2022, there were an estimated 20 million new cancer cases and 9.7 million cancer-related deaths globally across both sexes.[1] Among various cancers, female breast cancer is the second most commonly diagnosed, accounting for 11.6% of cases. Notably, female breast cancer is also responsible for 6.9% of all cancer-related deaths.[1]

Breast cancer is a multifactorial disease that can occur due to a multitude of factors. Despite its occurrence globally, its mortality, survival, and incidence rate fluctuate significantly among different countries, which may be caused by a multitude of factors, like environmental factors, lifestyle choices, genetic factors, and population structure.[2] The treatment of breast cancer consists of a variety of techniques administered through different combinations, such as chemotherapy, surgery, radiation, hormonal therapy, and radiation.[3] Chemotherapy is the most common systemic treatment modality for breast cancer either adjuvant or neoadjuvant.[4] Chemotherapy agents include carboplatin, cyclophosphamide, 5-fluorouracil/capecitabine, taxanes (paclitaxel, docetaxel), and anthracyclines (doxorubicin, epirubicin) are all applied together as part of treatment schemes.[3] However, these treatment modalities face significant limitations, including systemic toxicity, multidrug resistance, limited cytotoxicity against malignant cells, and poor solubility and permeability.[5,6]

Nanotechnology, the study of particles smaller than 100 nm, has emerged as a promising approach to overcoming these limitations.[7] Nanoparticles possess distinct physicochemical characteristics, including an extraordinarily high surface area, improved mechanical strength, and higher reactivity, that differentiate them from bulk materials. The process of nanoparticle synthesis requires the use of synthetic methods, including chemical, physical, and biosynthetic techniques.[7] Chemical approaches are costly and involve hazardous chemicals, such as capping and reducing agents, which may produce hazardous byproducts.[7,8] The choice of an environmentally friendly solvent, a suitable reducing agent, and a safe stabilising material are the three most important requirements for the synthesis of nanoparticles.[7] Green biosynthesis has been an alternative technique employed, utilising natural products such as plants, fungi, bacteria, algae, and other organisms.[7,9] Plant extracts contain phytochemicals that function as stabilising and reducing agents. Extracts are obtained from plant components such as roots, leaves, stems, seeds and fruits.[10] Nanoparticles have the ability to produce reactive oxygen species (ROS) or start signalling pathways that influence cell death, such as necrosis, apoptosis, and autophagy.[11] Therefore, it is crucial to understand the nanotoxicity mechanism of action of these nanotherapeutics through different methods, including cell viability assay, flow cytometry and more.

Vangueria infausta subsp *infausta* is a nutraceutical plant found in Africa (southern and eastern parts). *Vangueria infausta*, also commonly known as African wild medlar, is a small tree or shrub that can reach 3-7 meters, as shown in Figure 1a. This shrub has leaves that are green and oval in shape (Figure 1c). Its fruit is a shiny dark green (Figure 1c), and is almost spherical when young, turning light brown when ripe, as shown in Figure 1b.[12] It is traditionally used for conditions such as candidiasis, fever, wound healing, parasitic worms, snake bites, infertility, coughing, abdominal aches, chest complaints, and menstrual issues.[13,14] Recorded secondary metabolites found in *Vangueria* species include tannins, anthraquinones, terpenoids, flavonoids, phenols, anthocyanins, quinones, coumarins, glycosides, and alkaloids.[12,14] An emerging discipline with numerous important applications in the medicinal and environmental domains is the green production of nanoparticles. The primary goal of green synthesis is to reduce the use of harmful compounds by creating environmentally acceptable nanoparticles from biological materials such as plants and bacteria.[15] While many previous studies have utilised a variety of plant extracts for green AgNP synthesis and demonstrated their bioactivity, there is a lack of information concerning the anticancer activity of

*To whom correspondence should be addressed
Email: blassang@uj.ac.za

ISSN 1996-840X Online / South African Chemical Institute / http://saci.co.za/journal
© The Author(s) Published under a Creative Commons Attribution 4.0 International Licence (CC BY 4.0)
https://doi.org/10.17159/0379-4350/2026/v80se1a26

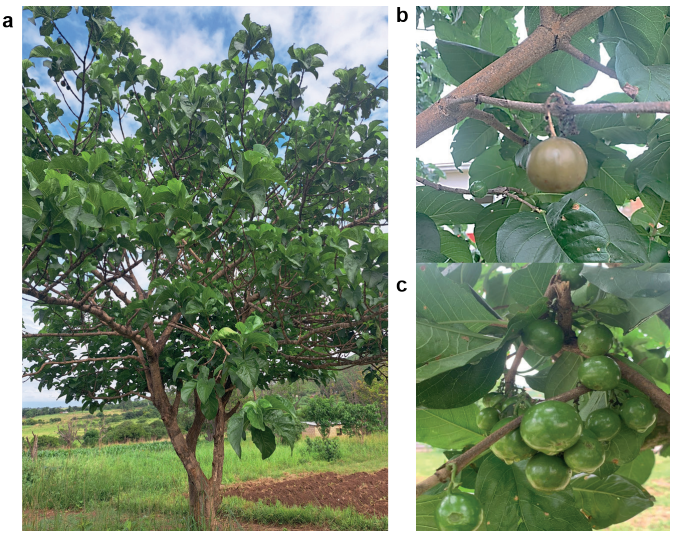


Figure 1: Images of *V. infausta* subsp. *Infausta* plant parts. (**a**) Mature shrub/tree (at 3-7 m in height), (**b**) Ripe fruit exhibiting characteristic light brown colouration at maturity and (**c**) Unripe fruit displaying shiny green, spherical and oval shaped leaves.

Vangueria infausta plant-mediated AgNP against triple negative breast cancer (TBNC). The mechanism of cell death against this aggressive subtype has not been investigated or characterised. Thus, the current study aimed to investigate the possibility of using *Vangueria infausta* leaf extract for AgNP synthesis as a novel reducing and capping agent, characterise its phytochemical properties, and investigate the cell death mechanism against TNBC.

METHODS AND MATERIALS

General Materials

Analytical-grade solvents and chemicals were used without further purification. The study used MDA-MB-231 (HTB-26) TNBC cells from the American Type Culture Collection (ATCC; Manassas, VA, USA). Hanks' balance salt solution (HBSS, 55037C, SIGMA® Life Sciences), fetal bovine serum (FBS, F0679, SIGMA® Life Sciences), high glucose Dulbecco's modified Eagle's medium (DMEM, D5796, SIGMA ® Life Sciences), and 0.25% TrypLE solution (Gibco™ 12563-029, ThermoFisher Scientific). Sigma-Aldrich provided high purity grade silver nitrate (209139), Penicillin-streptomycin (P4333), and Amphotericin B (A2942). CellTiter-Glo® reagent (G9682) and BD Pharmingen™ FITC Annexin V Apoptosis Detection Kit II (556570) were procured from Promega (Madison, WI, USA) and BD Biosciences (San Jose, CA, USA), respectively.

Plant extraction

The leaves of *V. infausta* were gathered from Warburton, Mpumalanga, South Africa (26°13′59″ S, 30°28′34″ E). They were washed with distilled water and left to dry in the shade for 8 weeks. A mortar and pestle were then used to crush the leaves into powder. About 10 g of crushed leaf powder was added in 100 mL of boiling distilled water for 15 min. The solution was left overnight (18–20 hours) and thereafter filtered through Whatman paper.

Nanoparticle synthesis

Plant extract (100 mg/mL) of 10 mL was mixed using a magnetic stirrer with 80 mL of 1 mM silver nitrate solution in Millipore water at 35 °C[16] for 6–10 hrs. Thereafter, the solution was placed in a centrifuge under specified conditions (10,000 rpm, 30 mins). The supernatant was then discarded, and the pelleted nanoparticles were washed twice with Millipore water. Nanoparticles were dried at rtp for 72 h.

UV-visible absorption spectrum

The UV-visible absorption spectrum was used to confirm AgNP formation. The green synthesised AgNPs were scanned from 220 to 800 nm at 1 nm wavelength intervals using a UV-vis spectrophotometer (Jenway 7315, Lasec, South Africa). An 850 µL volume of nanoparticles (3 mg/mL in 0.001 M PBS) was placed in a quartz cuvette (path length 1 cm) and measured. PBS was used as a dispersion medium to maintain physiological ionic strength and pH during measurement, ensuring reproducible absorbance readings.

Fourier transform infrared spectroscopy

Fourier transform infrared spectroscopy (FTIR) measurements were performed using the potassium bromide (KBr) pellet technique. Nanoparticles were frozen at -80 °C for 18 h and thereafter lyophilised for 72 h. The dried nanoparticles were ground into a fine powder, mixed with KBr, and then compressed into a pellet using a hydraulic press. The pellet was placed in an FTIR sample holder and analysed. This measurement was taken using a PerkinElmer Spectrum FTIR spectrometer over the mid-infrared range 400–4000 cm−1, with 25 scans.

Zeta potential and dynamic light scattering

The size and surface charge of the nanoparticles were analysed using a Malvern Zetasizer Nano ZS (software version 7.20), which features a 4 mW He-Ne laser with a wavelength of 633 nm. The set parameters for the samples were 25 °C, using 13° and 173°. Approximately 1 mg/mL of nanoparticle solution in distilled water at pH levels of 6.6 and 7.4 was added to a 3 x 3 mm Zeta dip cell cuvette with an integrated electrode, which was used to analyse the aforementioned characteristics.

Transmission electron microscope

A Transmission Electron Microscope (TEM, FEI Tecnai T12a) was utilised to analyse the size and morphology of nanoparticles. Nanoparticles resuspended in PBS were sonicated for 1 hour and then added onto carbon-coated 200-mesh copper grids (S-3620C-FA, SPI Suppliers) through a dropwise technique (5–20 µL). Sample-loaded grids are then left to dry overnight in the dark. The dried grids with the sample were loaded onto the appropriate sample placement on the microscope, and sample images were acquired.

Scanning electron microscopy and energy dispersive spectroscopy

Scanning electron microscopy (SEM) images of the AgNPs were acquired under the following conditions. The sample was carbon-coated and placed on a TESCAN SEM (software: Vega 3). SEM was operated in a controlled hydrogen chamber under vacuum at an acceleration voltage of 20 kV, a working distance of 15 mm, and utilising both backscatter electron and secondary electron detectors. Energy-dispersive spectroscopy (EDS) was used to determine the elemental composition of selected sections, utilising an Oxford detector equipped with INCA software.

Cell culture

Triple negative breast cancer cell line MDA-MB-231 was grown in supplemented high glucose Dulbecco's modified Eagle's medium (D5796, SIGMA® Life Sciences). Supplements included 10 % fetal bovine serum, Amphotericin B at 1 %, and Penicillin-Streptomycin at 1%. These cells were seeded at 2×10^5 cells in a 35 mm plate and incubated at 95% humidity, 5% carbon dioxide, and 37 °C throughout all experiments. Cells were grown overnight before treatment with silver nanoparticles (AgNP). Cells were treated at carrying

concentrations of AgNP (0-12 µg/mL) for 24 h, and further cell analysis was conducted. Untreated cells (no treatment) were included as a negative control to establish baseline viability.

Brightfield microscopy

Morphological changes observed after treatment were viewed under an inverted microscope with a digital camera attached (Olympus CKX41 and C5060-ADUS, respectively). Brightfield parameters were used to evaluate alterations in cell morphology using CellSens version 2.3 software.

Adenosine triphosphate assay

Luciferin contained in the CellTiter Glo® reagent binds to adenosine triphosphate (ATP) in lysed cells, which produces luminescence that can be read. After treatment, 100 µL of suspended cells in 1 x HBSS were added in an opaque 96-well plate. Thereafter, 100 µL CellTiter Glo® reagent (Promega, G9682) was also added to each well plate. The plate was placed in a shaker for 5 min and then incubated in the dark at room rtp for a further 25 min. A microplate reader (PerkinElmer, VICTOR Nivo™) was used to record the results of the plate. The untreated group was used to calculate the percentage of cell viability.

Annexin V/PI assay

BD Pharmingen™ FITC Annexin V Apoptosis Detection Kit II (556570) was used to analyse the proportion of live, apoptotic and necrotic cells following the treatment protocol. Cells were washed twice with cold PBS, then resuspended in 1X binding buffer. 100 µL of cell suspension was transferred into a 5 mL culture tube, and thereafter FITC Annexin V and PI (5 µL each) were added. Incubation was carried out at room temperature in the dark for 15 minutes, followed by the addition of 400 µL of 1X binding buffer. Stained cells were vortexed and analysed using a BD flow cytometer.

Statistical analysis

The data are presented as the mean ± standard deviation from three or more independent experiments performed in triplicate. The student t-test was used to compare data from various treatment groups with the untreated group (negative control). Data with a p-value of 0.05 or less was considered statistically significant. ($p < 0.05$ (*), $p < 0.01$ (**), or $p < 0.001$ (***)) indicates statistically significant differences between the mean values of the untreated and treated groups. Statistical analysis was carried out using nonlinear regression with a sigmoidal (dose-response) model, plotted on a semi-logarithmic scale. Confidence intervals of ≥95% were used to calculate IC_{50} and IC_{90} values.

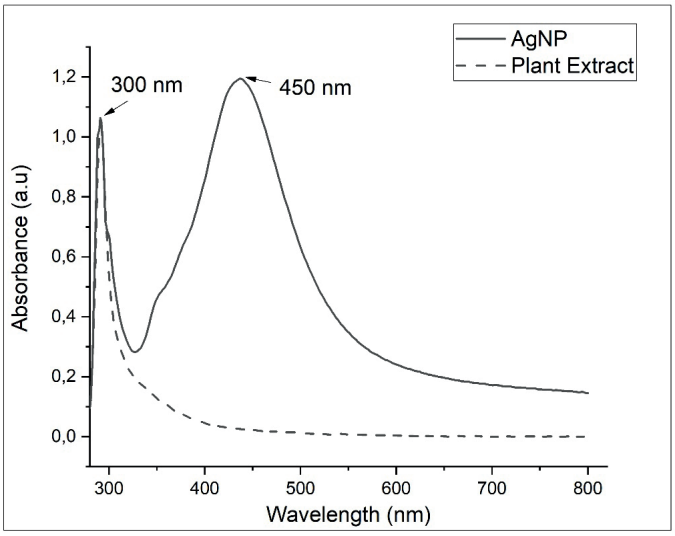


Figure 2: UV-Vis absorption spectrum of *V. infausta* leaf aqueous extract (dotted line) and green-synthesised nanoparticles (black line) in PBS at a spectral range of 200–800 nm. The plant extract showed a strong absorption peak at 300 nm, and the AgNP showed a prominent peak at 450 nm.

RESULTS AND DISCUSSION

UV-visible analysis

The absorption spectra of green-synthesised AgNPs in distilled water. These *V. infausta*-derived AgNPs show a strong absorption peak at 450 nm. AgNPs showed a prominent peak at 450 nm, as shown in Figure 2, thereby confirming their formation. This distinct peak can be attributed to their surface plasmon resonance (SPR). When exposed to incident light, the conduction-band electrons of the metal nanoparticles collectively oscillate, causing this effect. The shape, size, and aggregation feature of the nanoparticles affect the SPR peak intensity and location.[17] Similar to our study, the extract from *Azadirachta indica* leaves and *Curcuma longa* powder produced a peak at 440 nm,[17] which was also seen for the aquatic fungus *Saprolegnia parasitica* at 428 nm.[18]

Fourier transform infrared spectroscopy

The silver nanoparticles produced during green synthesis were evaluated, and the molecular structure and functional groups responsible for nanoparticle reduction, capping, and stabilisation were analysed.[19] Upon reviewing the results obtained from the FTIR spectrum (Figure 3) in the previously mentioned region, it was found that the O-H stretching vibrations are responsible for the absorption band at 3435.97 cm^{-1}. Metabolites found in that region are phenolic and alcoholic compounds.[20] The stretch vibration of the C-H group was observed in absorption bands at 2919.25 cm^{-1} and 2850 cm^{-1}.[21] These bands represent carbonyl compounds, esters, aldehydes, and ketones derived from tannins and flavonoids.[22] The stretching vibrations of the C=O group are observed at the absorption peak 1631.82 cm^{-1} and can be attributed to polysaccharide constituents and primary and secondary amide bonds in proteins. The absorption peak at 1049.41 cm^{-1} indicates C-N stretching in amines.[19,21] The presence of these functional groups confirms the involvement of phytochemicals in the reduction, capping, and stabilisation of AgNPs.

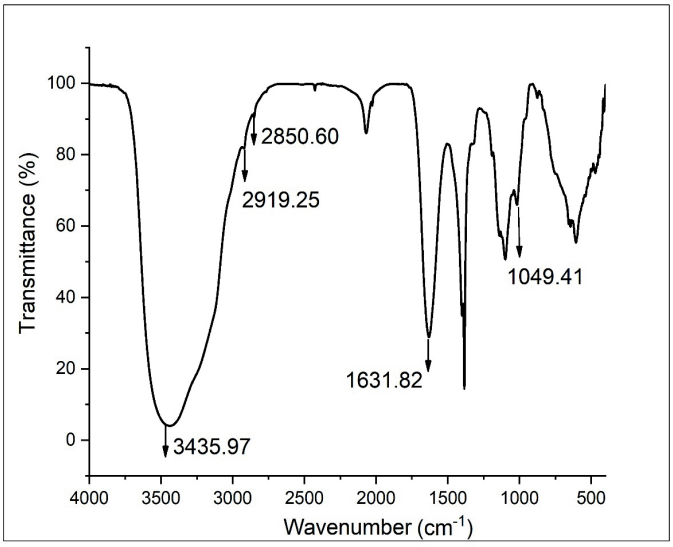


Figure 3: FTIR spectra graph of green synthesised nanoparticles showing functional groups expressed by AgNP derived from *V. infausta* aqueous extract. Characteristic absorption bands are observed at 3435.97 cm^{-1} (O-H stretching vibrations), 2919.25 cm^{-1} and 2850 cm^{-1} (C-H stretching of carbonyl compounds, esters, aldehydes, and ketones), 1631.82 cm^{-1} (C=O stretching vibrations of polysaccharides and proteins) and 1049.41 cm^{-1} (C-N stretching of amines)

Zeta potential and dynamic light scattering

Important details regarding the stability, size, and homogeneity of the generated AgNPs can be obtained by analysing zeta potential and size distribution (Figure 4). At pH of 6.6 and 7.4, the size distribution of AgNPs derived from *V. infausta* leaf extract was 172.0 and 173.7 d.nm, respectively (Figure 4a and b), while the zeta potential was -30.6 and -29.3 mV, respectively (Figure 4c and d). The zeta potential and DLS values are summarised in Table 1. The zeta potential was measured twice: at pH 7.4, which mimics the physiological environment (blood plasma and extracellular fluid),[23] and at pH 6.6, which imitates the tumour microenvironment (TME).[24] The acidity of TME is caused by the Warburg effect and hypoxia, leading to lactate accumulation. The pH range in TME is 6.5 to 6.8. It is crucial to evaluate the colloidal stability of the developed nanoparticles in this solution, as this will reflect their actual behaviour upon entering the bloodstream and tumour tissue.[25] Due to electrostatic repulsion, nanoparticles with a zeta potential value greater than 30 mV or less than – 30 mV are typically regarded as stable. Green-synthesised AgNPs have been found to be negatively charged. This is confirmed in studies completed by Ahani and Khatibzadeh,[26] Wang and colleagues,[27] and Kurra and colleagues.[28] The nature of the methods used can explain why the size measured by DLS is larger than the size observed in TEM (approximately 12.5 nm). DLS measures the hydrodynamic diameter, which encompasses the hydration shell, capping layer, and any related stabilising chemicals in addition to the core nanoparticle. TEM, on the other hand, directly shows the nanoparticle core, omitting the capping layer and solvent interactions. The notable variation demonstrates how the biomolecules in the Hordeum vulgare extract help to produce a stable shell around the nanoparticles. This investigation highlights the involvement of barley seed extract in the formation of nanoparticles with a hydrodynamically larger, stabilised structure (as shown by DLS) and a small core size (as confirmed by TEM), with modest colloidal stability as evidenced by the zeta potential test.[28]

Microscopy and elemental analysis

The use of electrons to magnify objects in TEM has allowed for the examination of the intricate internal architecture of objects at the nanoscale.[29] The TEM analysis of nanoparticles revealed a size range of 10-21 nm (Figure 5c), with an average length of 17.6 nm, as determined using ImageJ. Nanoparticles showed spherical orientation (Figure 5a), which was also reported in previous studies from plant-derived AgNPs such as *Ziziphus nummularia*[30] and *Aerva lanata*.[29] Flower extracts from the *Aerva lanata* plant morphological examination showed spherical, poly-dispersed biosynthesised AgNP that range from size 2 to 19 nm, while leaf extract from the *Ziziphus nummularia* plant showed spherical, homogenous shaped AgNPs which ranged in sizes from 33 to 89 nm.

SEM image analysis revealed spherical structures of nanoparticles. Figure 5c further showed the EDS spectrum absorption peak of AgNPs at 3 keV. Typically, AgNPs reported in previous studies are observed in the absorption peak range of 2 to 4 keV. Tannis extracted from *Vitis vinifera* pomace showed AgNPs with absorption peaks at 2.5–3.5 keV region.[31] A study using leaf extracts from *Coccinia grandis* presented EDS findings with a AgNP optimal peak at 3 keV.[32] In another study, which explored leaf extracts from different *Carica papaya, Ocimum gratissimum, Perilla frutescens, Achillea millefolium*, and *Garcinia kola* (nut extract), synthesised AgNPs showed a consistent absorption peak at 3 keV.[33]

Morphology and adenosine triphosphate assay

Secondary metabolites have been reported to have anticancer potential.[34] This is seen through their activity by targeting cancer cell signal pathways, thereby regulating antioxidants, enhancing apoptosis, and cell cycle arrest. Phytochemicals used in nanoformulations have the ability to enhance cellular uptake, target specific cells/tissues, improve therapeutic dosages, and enhance aqueous solubility and bioavailability.[35] A morphological analysis was completed whereby

Table 1: The mean values of the Zeta potential and DLS from AgNP derived from *V. infausta* aqueous extract.

pH	Zeta Potential (mV)	DLS (d.nm)
6.6	-29.3±4.46	173.7±114.0
7.4	-30.6±6.09	172.0±146.7

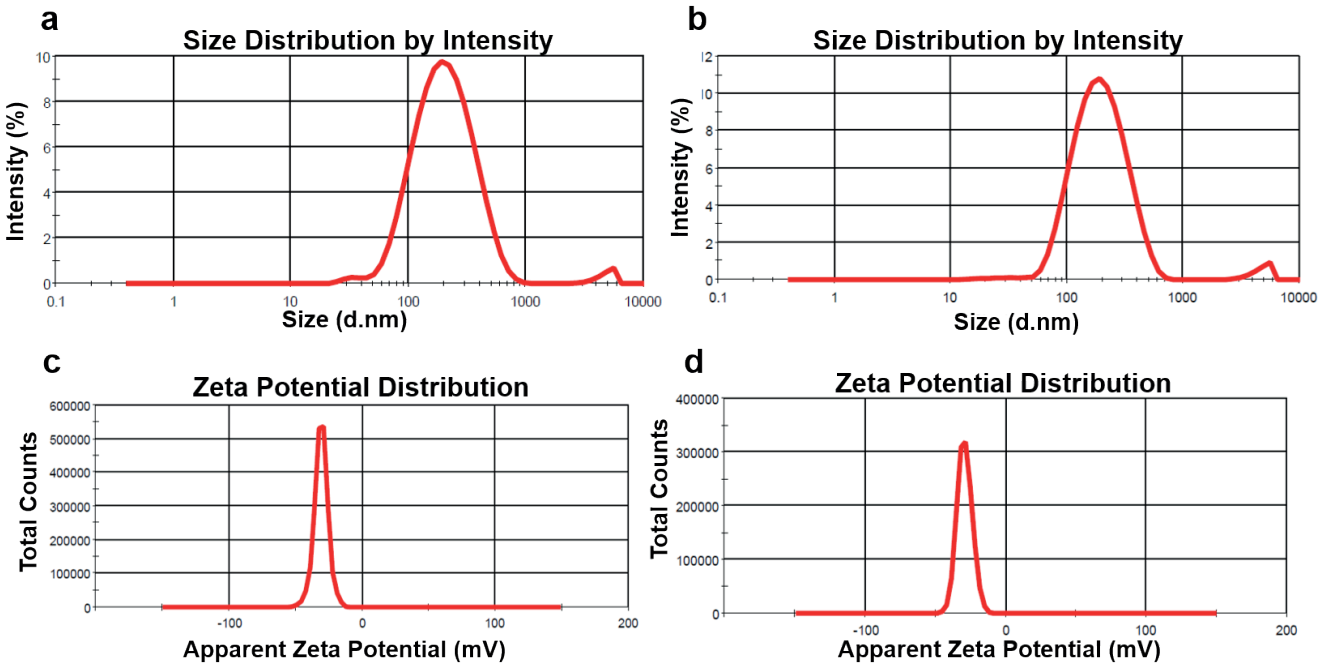


Figure 4: Hydrodynamic size distribution and zeta potential measurement of AgNP derived from *V. infausta* aqueous extract at different pH conditions relevant to biological environments. (**a**) size distribution at pH 6.6 (tumour environment mimic) showing a hydrodynamic diameter of 173.7 d.nm, (**b**) size distribution at pH 7.4 (physiological condition) showing 172 d.nm, (**c**) zeta potential at pH 6.6 at -29.3 mV, and (**d**) zeta potential at pH 7.4 at -30.6 mV. The negative charge indicates colloidal stability. Data represent mean ± SD from three measurements.

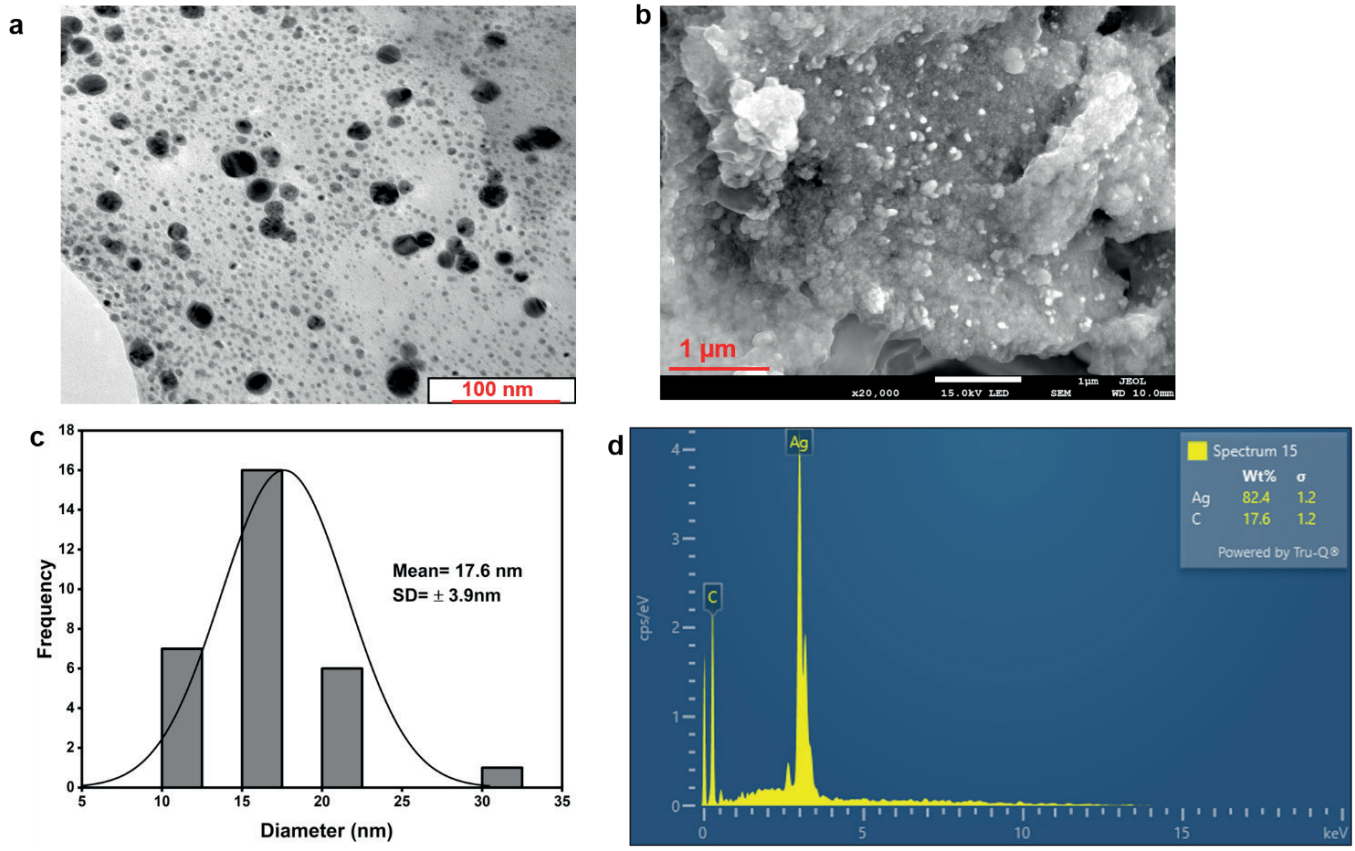


Figure 5: Morphological and elemental characteristics of AgNPs from *V. infausta*. **a** TEM image showing spherical nanoparticles (100 nm scale bar), (**b**) SEM image confirming spherical surface morphology (scale bar 1 µm), (**c**) size distribution histogram showing a mean diameter of 17.6±3.9 nm and (**d**) EDS spectrum showing silver (Ag) absorption peak at 3 keV and carbon at ~0.3 keV.

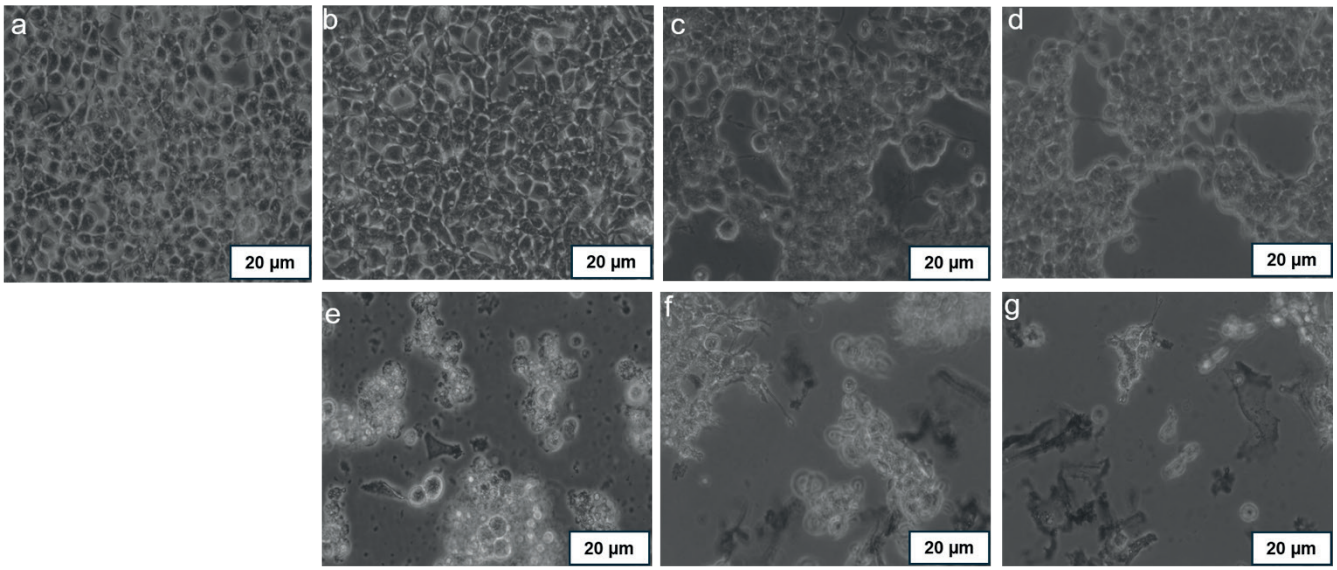


Figure 6: Brightfield microscopic images showing morphological alterations in MDA-MB-231 cells after 24 h AgNP treatment with increasing concentrations from 0-12 µg/mL (20 µm scale bar, 200X magnification). (**a**) untreated cells showing intact cellular membrane, (**b-g**) treatment at 2, 4, 6, 8, 10 and 12 µg/mL, respectively, showing cell, cell shrinkage, cell debris, and loss of adhesion.

MDA-MB-231 cells treated were compared to the untreated control group. Untreated cells showed intact cellular membrane and an elevated number of cells, while IC_{50} (Figure 6e) treated cells showed decreased cells, floating cells, cell shrinkage, and cell debris. Similar findings were observed when A549 lung cancer cells were treated with AgNP at 10-200 µg/mL.[36] MDA-MB-231 treated in a dose dependant manner at 2, 4, 6, 8, 10, 12 µg/mL. The IC_{50} of synthesized AgNP was found to be 5,4 µg/mL as shown in Figure 7b. Cell viability of triple negative cells was significantly reduced, confirming the cytotoxic effects of AgNP. *Allium sativum* L., *Camellia sinensis* L., and *Curcuma longa* L. were utilized in green synthesis and caused dose-dependent cytotoxicity to four cancer cell lines, cervical (HeLa), human breast adenocarcinoma (MCF-7), lung (A549), human dermal fibroblast (NHDF), and epithelioma (Hep2). Their IC_{50} after of these green synthesized nanoparticles from *Allium sativum* L., *Camellia sinensis* L. and *Curcuma longa* L. on MCF-7 specifically was (19.94, 20.97, and 11.65 µg/mL, respectively).[37] In comparison with our plant, these green synthesized nanoparticles required higher concentrations to

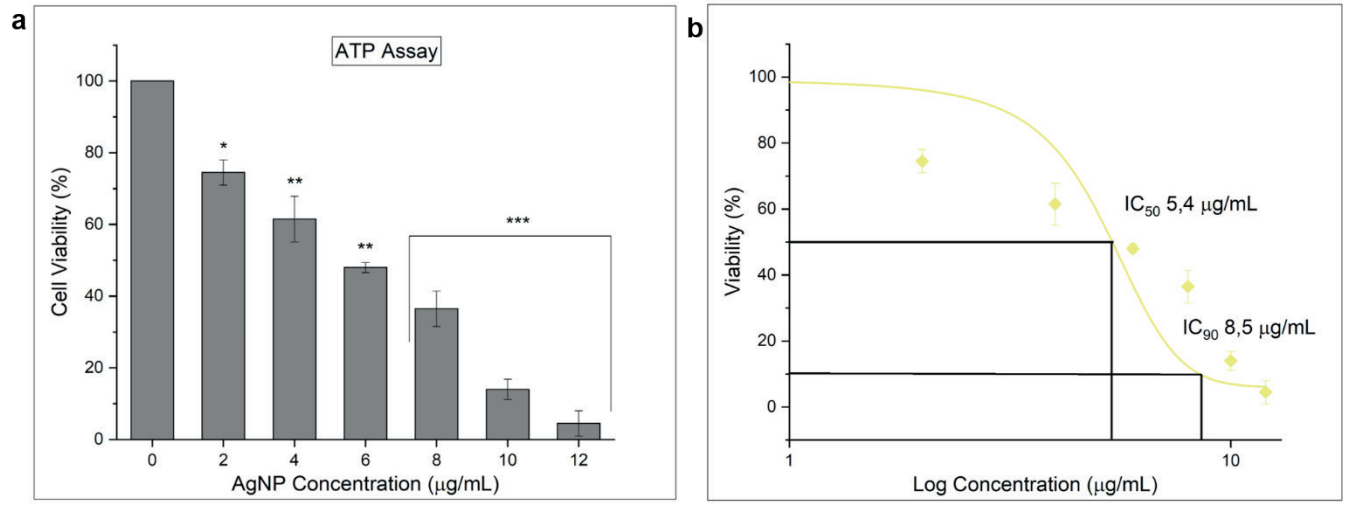


Figure 7: Cytotoxic effects of MDA-MB-231 cells after 24 h AgNP treatment at 2-12 µg/mL, (**a**) bar graph and (**b**) dose response curve. The significant difference between the untreated and treated mean values are shown by (p <0.05 (*), p < 0.01 (**) or p <0.001 (***)).

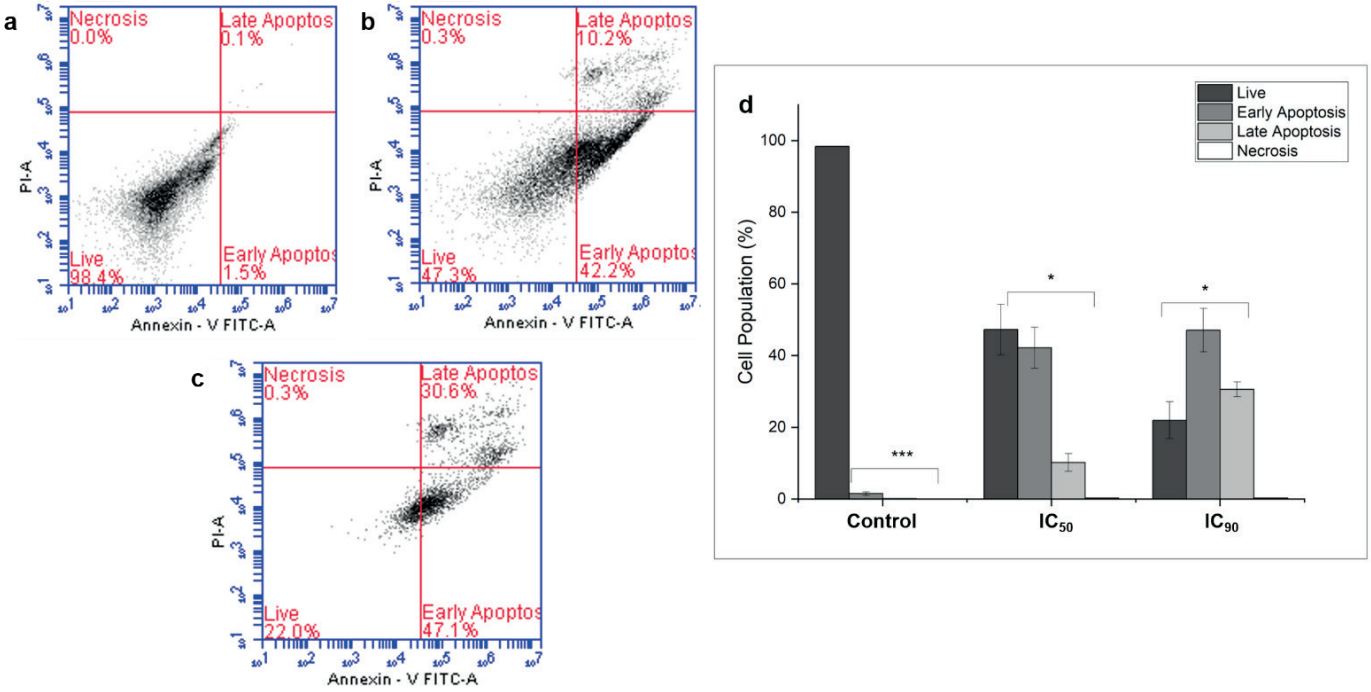


Figure 8: Flow cytometry analysis of cell death mechanism found in MDA-MB-231 cells after 24 h AgNP treatment using FITC-Annexin V/PI dual staining. Representative dot plots showing viable cells, apoptosis and necrosis. (**a**) untreated MDA-MB-231 cells with ~98.4% viable cells, (**b**) IC_{50} 5.4 µg/mL showing ~47.3% viable cells, (**c**) IC_{90} 8.5 µg/mL with ~22% viable cells and (**e**) bar graph representing percentage of live, apoptotic (early and late) and necrotic cell populations for all experimental groups. Results showed the main cell death pathway as apoptosis. The significant difference between the untreated and treated mean values are shown by (p <0.05 (*), p < 0.01 (**) or p <0.001 (***)).

effectively induce significant cancer cell death. In another study with green synthesized nanoparticles using chitosan found an IC_{50} of MCF-7 and MDA-MB-231 cancer cell lines was 6.4 and 6.56 ppb.[38] This study was found to be comparable to our study against triple-negative breast cancer cells using *V. infausta*.

Cell death analysis

The investigation of AgNP against MDA-MB-231 breast cancer cells, which induced apoptosis, was carried out using flow cytometry. Treatment of these cells at different concentrations resulted in varying percentages of live, apoptotic (early and late), and necrotic cells (Figure 8d). The live cells untreated with AgNP showed 98% viability of cells (Figure 8a), while treatment groups at 5.4 µg/mL showed live cells at 47%, early apoptotic cells at 42% and late apoptotic cells at 10% (Figure 8b) and at 8.5 µg/mL showed live cells at 22%, early apoptotic cells at 47% and late apoptotic cells at 30% (Figure 8c). This shows that the cell death mechanism triggered by AgNP in this study is through apoptosis. In a study against colorectal cancer, green-synthesised AgNPs using *Allium cepa* L showed a ~29 and ~89 % induction of apoptosis at 10 and 20 µg/mL.[39] In another study, the *Fagonia indica* plant was used to synthesise AgNPs against breast cancer cells (MCF-7 cell line) 12.35 µg/mL treatment showed early apoptotic cells at ~43% and late apoptotic cells at ~24%.[40] These studies further confirm that the primary mechanism of cell death induced by green-synthesised AgNPs is apoptosis. Critically, it was found that the use of this particular plant species resulted in the substantial induction of cell death in TNBC cells, demonstrating for the first time the potential anticancer activity of this poorly studied plant, which may serve as the basis for further research into the mechanisms of action, toxicity, as well as preclinical and clinical studies.

CONCLUSION

The data obtained from this study demonstrate the successful synthesis of AgNPs using the leaf extract of *V. infausta*. The compounds extracted from this plant facilitated the reduction, capping, and stabilisation of the produced nanoparticles. UV-Vis spectroscopy confirmed the presence of AgNPs, while FTIR, TEM, SEM, EDS, and zeta potential measurements revealed the typical characteristics of stable AgNPs. These synthesised nanoparticles exhibited reduced cell viability and induced apoptosis in TNBC cells. The findings establish that AgNPs derived from *V. infausta* hold promise as a platform for further anticancer research. Additional models are necessary to elucidate the molecular pathways involved in apoptotic induction, evaluate in vivo efficacy and toxicity in preclinical models, and explore potential applications in drug delivery. This study lays the groundwork for these future investigations.

SUPPLEMENTARY INFORMATION

There is no Supplementary Information associated with this manuscript.

ACKNOWLEDGMENTS

The authors sincerely thank the South African Research Chairs initiative of the Department of Science and Technology; the National Research Foundation (NRF) of South Africa [Grant No. 98337]; the South African Medical Research Council [Grant No. SAMRC EIP007/2021], as well as grants received from the NRF Research Development Grants for Y-Rated Researchers [Grant No. 137788]; University Research Committee (URC); African Laser Centre (ALC) (Grant No. HLHA26X Task ALC-R001); University of Johannesburg, and the Council for Scientific Industrial Research (CSIR)-National Laser Centre (NLC) for funding. The University of Johannesburg, Faculty of Health Sciences Higher Degree Committee (HDC-01-27-2024) and Research Ethics Committee (REC-2702-2024) for ethics approval.

CREDIT AUTHORSHIP CONTRIBUTION STATEMENT

Conceptualization, N.T.F. and B.P.G.; writing—original draft preparation, N.T.F.; writing—review and editing, B.P.G. and H.A.; supervision, B.P.G. and H.A. All authors have read and agreed to the published version of the manuscript.

DECLARATION OF COMPETING INTEREST

The authors declare that they have no known competing financial interests.

DECLARATION OF GENERATIVE AI AND AI-ASSISTED TECHNOLOGIES

ScholarAi and Grammarly were used to improve readability and language. After using the AI tool, the authors reviewed and edited the content again and take responsibility for content published in this article.

AUTHOR ORCID IDS

Nosipho T. Fakudze: https://orcid.org/0000-0003-3686-4209
Heidi Abrahamse: https://orcid.org/0000-0001-5002-827X
Blassan P. George: https://orcid.org/0000-0003-0700-9246

REFERENCES

1. Bray F, Laversanne M, Sung H, Ferlay J, Siegel RL, Soerjomataram I, Jemal A. Global cancer statistics 2022: globocan estimates of incidence and mortality worldwide for 36 cancers in 185 countries. CA Cancer J Clin. 2024;74(3):229–263. https://doi.org/10.3322/caac.21834.
2. Momenimovahed Z, Salehiniya H. Epidemiological characteristics of and risk factors for breast cancer in the world. Breast Cancer (Dove Med Press). 2019;11:151–164. https://doi.org/10.2147/BCTT.S176070.
3. Łukasiewicz S, Czeczelewski M, Forma A, Baj J, Sitarz R, Stanisławek A. Breast cancer—epidemiology, risk factors, classification, prognostic markers, and current treatment strategies—an updated review. Cancers (Basel). 2021;13(17):4287. https://doi.org/10.3390/cancers13174287.
4. Obidiro O, Battogtokh G, Akala EO. Triple negative breast cancer treatment options and limitations: future outlook. Pharmaceutics. 2023;15(7):1796. https://doi.org/10.3390/pharmaceutics15071796.
5. Sartaj A, Baboota S, Ali J. Nanomedicine: A promising avenue for the development of effective therapy for breast cancer. Curr Cancer Drug Targets. 2020;20(8):603–615. https://doi.org/10.2174/1568009620666620033124113.
6. Zhang Z, Lim D, Feng Z. A review of therapeutic agents for breast cancer with potentially radiosensitizing properties. Radiat Med Prot. 2024;5(2):75–82. https://doi.org/10.1016/j.radmp.2024.03.002.
7. Jadoun S, Arif R, Jangid NK, Meena RK. Green synthesis of nanoparticles using plant extracts: A review. Environ Chem Lett. 2021;19(1):355–374. https://doi.org/10.1007/s10311-020-01074-x.
8. Chakraborty P, Khatiwara B, Singh S, Sarangi S, Das A, Dhakal J. Application of plant extracts for the synthesis of nanoparticles in green chemistry: A concise update. Curr Nanomater. 2023;8(3):224–232. https://doi.org/10.2174/2405461507666220531111906.
9. Kirubakaran D, Wahid JBA, Karmegam N, Jeevika R, Sellapillai L, Rajkumar M, Senthilkumar KJ. A comprehensive review on the green synthesis of nanoparticles: advancements in biomedical and environmental applications. Biomed Mater Devices. 2026;4(1):388–413. https://doi.org/10.1007/s44174-025-00295-4.
10. Ayub A, Wani AK, Malik SM, Ayub M, Singh R, Chopra C, Malik T. Green nanoscience for healthcare: advancing biomedical innovation through eco-synthesized nanoparticle. Biotechnol Rep (Amst). 2025;47:e00913. https://doi.org/10.1016/j.btre.2025.e00913.
11. Mohammadinejad R, Moosavi MA, Tavakol S, Vardar D, Hosseini A, Rahmati M, Dini L, Hussain S, Mandegary A, Klionsky DJ. Necrotic, apoptotic and autophagic cell fates triggered by nanoparticles. Autophagy. 2019;15(1):4–33. https://doi.org/10.1080/15548627.2018.1509171.
12. Nemapare P, Mugadza DT, Gadaga TH. Characterization of functional properties and organic acids invangueria infausta burch. (wild medlar/nzvirumombe/umviyo)fruit(s) found in zimbabwe. Int J Food Sci. 2025;2025(1): 9925294. https://doi.org/10.1155/ijfo/9925294.
13. Ngubane SC, Mbhele Z, Ntuli NR. Indigenous knowledge and traditional uses of vangueria infausta subsp. Infausta burch in northern kwazulu-natal, south africa. Plants. 2025;14(12):1820. https://doi.org/10.3390/plants14121820.
14. Maroyi A. Nutraceutical and ethnopharmacological properties of vangueria infausta subsp. Infausta. Molecules. 2018;23(5):1089. https://doi.org/10.3390/molecules23051089.
15. Maluleke MK, Ralulimi TS, Machete M. Biochemical constituents and the role of african wild medlar (vangueria infausta) in human nutrition: A review. Discov Sustain. 2024;5(1):37. https://doi.org/10.1007/s43621-024-00219-0.
16. Mariwowo E. Green sythesis of silver nanoparticles using vangueria infausta and parinaricuratellifolia leaf extract and evaluation on their antifungal activities. BSc(Hons) thesis, Midlands State University, Zimbabwe; 2017.
17. Kumar Singh R, Nallaswamy D, Rajeshkumar S, Varghese SS. Green synthesis of silver nanoparticles using neem and turmeric extract and its antimicrobial activity of plant mediated silver nanoparticles. J Oral Biol Craniofac Res. 2025;15(2):395–401. https://doi.org/10.1016/j.jobcr.2025.02.005.
18. Ali Habeeb Al-Khuzai R, Khadhim Aboud M, Khoman Alwan S. Biological synthesis of silver nanoparticles from saprolegnia parasitica. J Phys Conf Ser. 2019;1294(6):062090. https://doi.org/10.1088/1742-6596/1294/6/062090.
19. Pasieczna-Patkowska S, Cichy M, Flieger J. Application of fourier transform infrared (ftir) spectroscopy in characterization of green synthesized nanoparticles. Molecules. 2025;30(3):684. https://doi.org/10.3390/molecules30030684.
20. Gul A, Wahab A, Fozia F, Shah SM, Gul R, Ali J, Khan NR, Ahmad I, Ahmad N, Zia M, et al. Protein kinase inhibition, antibacterial activity, and characterization of phytoextract-mediated silver nanoparticles using aqueous extracts of ifloga spicata. J Nanomater. 2022;2022(1): 4447857. https://doi.org/10.1155/2022/4447857.

21. Melkamu WW, Bitew LT. Green synthesis of silver nanoparticles using hagenia abyssinica (bruce) j.F. Gmel plant leaf extract and their antibacterial and anti-oxidant activities. Heliyon. 2021;7(11):e08459. https://doi.org/10.1016/j.heliyon.2021.e08459.
22. Ragavendran P, Sophia D, Arul Raj C, Gopalakrishnan V. Functional group analysis of various extracts of aerva lanata (l.,) by ftir spectrum. Pharmacologyonline. 2011;1:358–364.
23. Padilha Lorenzett AK, Babinski TP, De Lima VA, Mainardes RM. Optimization of eudragit rs100 nanocapsule formulation for encapsulating perillyl alcohol and temozolomide using design of experiments. ACS Nanosci Au. 2025;5(2):70–83. https://doi.org/10.1021/acsnanoscienceau.4c00057.
24. Nogueira-Librelotto DR, Scheeren LE, Macedo LB, Vinardell MP, Rolim CMB. Ph-sensitive chitosan-tripolyphosphate nanoparticles increase doxorubicin-induced growth inhibition of cervical hela tumor cells by apoptosis and cell cycle modulation. Colloids Surf B Biointerfaces. 2020;190:110897. https://doi.org/10.1016/j.colsurfb.2020.110897.
25. Lane LA, Qian X, Smith AM, Nie S. Physical chemistry of nanomedicine: understanding the complex behaviors of nanoparticles in vivo. Annu Rev Phys Chem. 2015;66(1):521–547. https://doi.org/10.1146/annurev-physchem-040513-103718.
26. Ahani M, Khatibzadeh M. Green synthesis of silver nanoparticles using gallic acid as reducing and capping agent: effect of ph and gallic acid concentration on average particle size and stability. Inorganic and Nano-Metal Chemistry. 2022 Jan 13;52(2):234–240. https://doi.org/10.1080/24701556.2021.1891428.
27. Wang L, Wu Y, Xie J, Wu S, Wu Z. Characterization, antioxidant and antimicrobial activities of green synthesized silver nanoparticles from psidium guajava l. Leaf aqueous extracts. Mater Sci Eng C. 2018;86:1–8. https://doi.org/10.1016/j.msec.2018.01.003.
28. Gupta P, Ilyas H, Raghav DS, Tomar S. Sustainable synthesis of silver nanoparticles via hordeum vulgare seed extract: Catalysis, antioxidant, anti-cancerous and antimicrobial potential. Discov Mater. 2025;5:143. https://doi.org/10.1007/s43939-025-00342-3.
29. Palithya S, Gaddam SA, Kotakadi VS, Penchalaneni J, Golla N, Krishna SBN, Naidu CV. Green synthesis of silver nanoparticles using flower extracts of aerva lanata and their biomedical applications. Part Sci Technol. 2022;40(1):84–96. https://doi.org/10.1080/02726351.2021.1919259.
30. Golla N. Phytosynthesis and antimicrobial studies of silver nano particles using ziziphus nummularia leave extracts. MOJ Drug Design Development & Therapy. 2018;2(5):261–264. https://doi.org/10.15406/mojddt.2018.02.00056.
31. Hashim N, Paramasivam M, Tan JS, Kernain D, Hussin MH, Brosse N, Gambier F, Raja PB. Green mode synthesis of silver nanoparticles using vitis vinifera's tannin and screening its antimicrobial activity / apoptotic potential versus cancer cells. Mater Today Commun. 2020;25:101511. https://doi.org/10.1016/j.mtcomm.2020.101511.
32. Arunachalam R, Dhanasingh S, Kalimuthu B, Uthirappan M, Rose C, Mandal AB. Phytosynthesis of silver nanoparticles using coccinia grandis leaf extract and its application in the photocatalytic degradation. Colloids Surf B Biointerfaces. 2012;94:226–230. https://doi.org/10.1016/j.colsurfb.2012.01.040.
33. Kah G, Adelusi OA, Gbashi S, Awafong PM, Njobeh PB. Antifungal and antimycotoxin activity of plant-synthesized silver nanoparticles (AgNPs): A novel approach to combat food contamination. Food Microbiol. 2026;135:104979. https://doi.org/10.1016/j.fm.2025.104979.
34. Xia Y, Chen R, Lu G, Li C, Lian S, Kang T-W, Jung YD. Natural phytochemicals in bladder cancer prevention and therapy. Front Oncol. 2021;11:652033. https://doi.org/10.3389/fonc.2021.652033.
35. Rizwanullah M, Amin S, Mir SR, Fakhri KU, Rizvi MMA. Phytochemical based nanomedicines against cancer: current status and future prospects. J Drug Target. 2018;26(9):731–752. https://doi.org/10.1080/1061186X.2017.1408115.
36. Lee YS, Kim DW, Lee YH, Oh JH, Yoon S, Choi MS, Lee SK, Kim JW, Lee K, Song C-W. Silver nanoparticles induce apoptosis and g2/m arrest via pkcζ-dependent signaling in a549 lung cells. Arch Toxicol. 2011;85(12):1529–1540. https://doi.org/10.1007/s00204-011-0714-1.
37. Arumai Selvan D, Mahendiran D, Senthil Kumar R, Kalilur Rahiman A. Garlic, green tea and turmeric extracts-mediated green synthesis of silver nanoparticles: Phytochemical, antioxidant and in vitro cytotoxicity studies. J Photochem Photobiol B. 2018;180:243–252. https://doi.org/10.1016/j.jphotobiol.2018.02.014.
38. Bandyopadhyay A, Roy B, Shaw P, Mondal P, Mondal MK, Chowdhury P, Bhattacharya S, Chattopadhyay A. Cytotoxic effect of green synthesized silver nanoparticles in mcf7 and mda-mb-231 human breast cancer cells in vitro. Nucleus (Calcutta). 2020;63(2):191–202. https://doi.org/10.1007/s13237-019-00305-z.
39. Abdellatif AAH, Mahmood A, Alsharidah M, Mohammed HA, Alenize SK, Bouazzaoui A, Al Rugaie O, Alnuqaydan AM, Ahmad R, Vaali-Mohammad M-A, et al. Bioactivities of the green synthesized silver nanoparticles reduced using allium cepa l aqueous extracts induced apoptosis in colorectal cancer cell lines. J Nanomater. 2022;2022(1):1746817. https://doi.org/10.1155/2022/1746817.
40. Ullah I, Khalil AT, Ali M, Iqbal J, Ali W, Alarifi S, Shinwari ZK. Green-synthesized silver nanoparticles induced apoptotic cell death in mcf-7 breast cancer cells by generating reactive oxygen species and activating caspase 3 and 9 enzyme activities. Oxid Med Cell Longev. 2020;2020:1–14. https://doi.org/10.1155/2020/1215395.